Novel Distortion Compensation Scheme for Multichannel Direct RF Digitization Receiver

Ngoc-Anh Vu
Le Quy Don Technical University
Ha Noi, Viet Nam
ngocanh220484@gmail.com

Hai-Nam Le*
Le Quy Don Technical University
Ha Noi, Viet Nam
namlh@lqdtu.edu.vn
**corresponding author*

Thi-Hong-Tham Tran
Moscow Institute of Physics and Technology
Moscow, Russia
tranhongtham@phystech.edu

Quang-Kien Trinh
Le Quy Don Technical University
Ha Noi, Viet Nam
kien.trinh@lqdtu.edu.vn

***Abstract*—This paper presents the analysis of the nonlinear distortion model of Low Noise Amplifier (LNA) for direct RF digitization receivers (DRF–RX) and proposes a novel compensation technique for receivers working in multi-channel mode[1]. With the proposed design the distortion is suppressed by using a linear reference receiver with a least mean square (LMS) filter. As the major advantage, the distortion suppression is performed after the down-converter so all high-order distortion components are automatically phased out. Furthermore, as the signal is fully processed at a low sampling rate, our proposed scheme is much simpler and the circuit inherently consumes less energy and is more compact, compared to the prior arts.**

To demonstrate the proposed technique, a direct RF digitization UHF receiver with QPSK modulation has been built and modeled in Matlab. The simulation results show that we could achieve an improvement of ~30 dB in signal SFDR (Spurious-free dynamic range) with the standard two-tone test case, and a reduction of 1000 times in the bit-error-rate (BER) in comparison with the non-compensation receiver.

Keywords— Direct RF digitization, DCR, LNA distortion, digital receiver, LMS filter, multichannel receiver, software-defined radio, UHF transceiver.

I. INTRODUCTION

Direct RF digitization receiver (DRF–RX) is an increasingly popular architecture among receiver designs thanks to the advances in technology and it has been widely adopted in many commercial devices [1, 2]. Being all digital, this architecture permits substantially simplify the receiver structure, enables energy-saving and easy functionality upgrade. Besides, with the flexibility of the digital design, DRF–RX is a true software-defined RX that supports a wide range of operation modes, multiple bands, and multiple channels [1]–[6]. Last but not least, the all-digital architecture helps to overcome some permanent drawbacks coming from the analog components, e.g., there is no I/Q imbalance distortions or DC offset component caused by the analog quadrature mixers as in the conventional direct conversion receivers (DCRs) [3], [7].

Nonetheless, DRF-RX still suffers from the distortions originated from the LNA nonlinearity when working in multi-channel mode. Specifically, the multi-channel receiver allows the simultaneous recording of multiple channels with different types of signal modulation and power levels [9]-[13]. In such a condition, it is inevitable that after being amplified by the LNA, high energy channels generate nonlinear distortions. These distortions, in turn, degrade the signal quality of the nearby channels [9]–[13]. The higher the power of distortion channels, the more serious the effect of LNA nonlinearity is, and this essentially requires advanced technique and post-processing algorithms in the digital domain.

The studies in [9]–[13] proposed some solutions to reduce the distortion for DRF-RX. These studies all use either Hammerstein's model [10]–[13] or Volterra series [9] to mathematically characterize the LNA nonlinearity. In general, there are two basic solutions for distortion compensation: canceling or inverting all the nonlinear effects to extract the useful signal. Accordingly, the fundamental task is to reproduce and/or to estimate the distortion components from the received signal. Both solutions in [9] and [13] use a band-pass filter (BPF) for the distortion estimation. In [12], the distortion is evaluated using a part of distorted information from the variable high-frequency BPF. The main limitations of this method when using such a variable high-frequency BPF are the incomplete distortion reproduction, the technological complexity, and the implementation cost increase. Similarly, authors in [13] used a BPF to extract the distortion signals. However, this compensation technique is not "blind", as the channel's frequency and bandwidth information have to be known in advance. A solution using a secondary reference receiver to reproduce and suppress distortion is proposed in [10]. However, the distortion compensation is carried out at the high-frequency domain and the technique was applied for common DCRs with existing non-linear distortion components from the analog sub-circuit (i.e., quadrature mixers). Thus, the compensation circuit was highly complex and energy-consuming.

In this work, we propose a novel distortion compensation for multichannel DRF-RXs. The primary difference between

[1] Multichannel DRF-RX is a receiver that allows the reception of channels with a frequency range at a time.

our technique and prior arts is that the proposed compensation circuit works at baseband rather than in intermediate or radio frequency (RF) domains. In such a manner, this design has twofold advantages. First, the digital down-converter (DDC) acts as a low-pass filter (LPF), which eventually filters out most of the high-order distortion components (i.e., these harmonics locate far-away from the interested bandwidth), among them all are even-order harmonics. Second, as all processes are at the low-frequency domain, the complexity and design cost are significantly reduced. In other words, the proposed technique simultaneously helps improve the receiver power profile and lessen the demand on the sample buffer. Hence, our proposed design is suited for a wide range of applications, especially for battery-back and handheld devices where energy consumption and achieving design compactness are critical. A case study using a UHF-range QPSK receiver shows that our proposed compensation circuit responses fast enough to the input changes, helps improve the signal SFDR and reduces the BER significantly.

The remaining of the paper is organized as follows. Section II presents distortion models of LNA and analyzes the effect of distortion on the multichannel DRF-RX model. Section III proposes the solution to compensate LNA's distortions. Conclusions are drawn in section IV.

II. NONLINEAR LNA DISTORTIONS MODELS IN DRF-RXS

A. RF Nonlinear Distortion Model

The generic structure of DRF-RX is shown in Fig. 1. An array of BPFs is still required in order to attenuate the out-of-band frequencies [3]. Then, the filtered signal is going through an LNA before being digitalized by a high-speed ADC. From the practical point of view, the resolution of the state-of-the-art ADCs, which is suitable for DRF-RX, is only about 14 bits [15, 16], which corresponds to an approximate SFDR of 86 dB [18]. To ensure the receiver sensitivity of approximate -100 dBm, the signal would need to be amplified by about 20 dB. Hence, the LNA is an indispensable component in any DRF-RX designs [3], [13]. Unfortunately, the LNAs only work linearly with a limited input power range. When the input signal energy is higher than the linear threshold, the amplifier becomes saturated and nonlinear distortions appear at the amplifier output [3]-[14]. There are two types of nonlinear LNA distortions that need to be taken into consideration: self-affected distortions caused by an individual RF signal to itself and distortions causes by the interference of other RF signals [3], [14]. The model of nonlinear components is assumed to be a polynomial with the form

$$y_{RF}(t) = a_1(t)x_{RF}(t) + a_2(t)x_{RF}^2(t) + a_3(t)x_{RF}^3(t) + \cdots + a_n(t)x_{RF}^n(t) \quad (1),$$

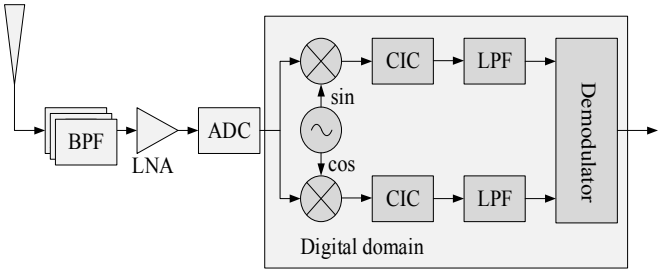

Fig. 1. The architecture of direct digitization receiver

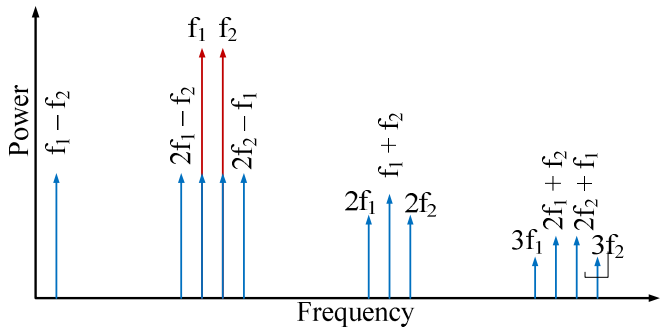

Fig. 2. The nonlinear components of LNA with two-tone input

where $x_{RF}(t)$ and $y_{RF}(t)$ are LNA input and output signals respectively; $a_i(t)$ is the i[th]-order component coefficient. The input signal $x_{RF}(t)$, in turn, is represented as

$$x_{RF}(t) = 2Re[x(t)e^{j\omega_c t}] = x(t)e^{j\omega_c t} + x^* e^{-j\omega_c t} \quad (2),$$

where $x(t)$ is the baseband signal of $x_{RF}(t)$, $x(t)$ can be a single carrier frequency or multiple separate carrier frequencies. $\omega_c = 2\pi f_c$, with f_c is the center carrier frequency and (.)* represents complex conjugate.

As illustrated in Fig. 2, when the input signal has two frequencies components (f_1, f_2), the output signal will have two harmonic groups: $n \times f_1$, $m \times f_2$, and inter-modulation $n \times f_1 \pm m \times f_2$. The distortion happens as soon as those components appear near the received signal frequency. For example, components $(2f_1 - f_2)$ and $(2f_2 - f_1)$ could distort f_1 and f_2. The other harmonics and inter-modulation, on the other hand, could distort other high-frequency signals.

B. Baseband Nonlinear Distortion Model

With the DRF-RX structure shown in Figure 1, assume that $2f_c \gg BW$ (bandwidth), a significant number of out-of-band signals will be removed after the digital downconverters. This is because the DDC acts as an LPF, which shifts the RF signal to the baseband. Correspondingly, the expression of (1) can be greatly simplified. The quadratic component in (1) is expressed as

$$x_{RF}^2(t) = 2A(t) + x^2(t) \cdot e^{2\omega_c t} + [x^*(t)]^2 \cdot e^{-j2\omega_c t} \quad (3)$$

where $A^2(t) = x(t) \cdot x^*(t)$ is the spectral content around the DC component. From (3), distortion frequencies appear at 0 and $\pm 2\omega_c$but there is no frequency component at ω_c. Similar

discussion can be found for other even order components. Therefore, all even-order harmonics in (1) are eventually phased out after the DDC. Similarly, other high-frequency distortion components will not appear at reception bandwidth and can be excluded.

Therefore, in DRF-RXs, LNA's non-linearity is most severe at only odd-order components because their generated distortions could locate around ω_c. In practice, it is sufficient to take into consideration up to the third-order components because higher-order components often have very small energy [22].

Therefore, the simple RF non-linear model can be written as

$$y_{RF}(t) = a_1 x_{RF}(t) + a_3 x_{RF}^3(t) \tag{4}$$

Here a_1 is the linear gain of LNA, and a_3 is the distortion coefficient of the third-order component. The impact of LNA non-linearity distortion components affecting DRF-RX is illustrated in Fig. 3. As can be seen from the figure, the third-order intermodulation of f_1, f_2 produce frequencies (i.e., $2f_1 - f_2$, $2f_2 - f_1$), which are closed to f_3, f_4 and f_5 interfere channels at these positions. Higher harmornic and intermodulation are filtered out at moderate BW of the UHF receiver

From (2), the third-order component in (4) can be written in full form as

$$\begin{aligned} &a_3 x_{RF}^3(t) \\ &\quad = a_3\{x^3(t)e^{j3\omega_c t} + [x^*(t)]^3 \cdot e^{-j3\omega_c t} + 3A^2(t) \\ &\quad \cdot x(t)e^{j\omega_c t} + 3A^2(t)x^*(t)e^{-j\omega_c t}\} \end{aligned} \tag{5}$$

After I/Q downconversion, all high-frequency components (at $3\omega_c$) are removed, the remaining components in (5) is $3A^2(t) \cdot x(t) \cdot e^{j\omega_c t}$ and $3A^2(t) \cdot x^*(t) \cdot e^{-j\omega_c t}$. Hence, the baseband equivalence of the LNA non-linear model for DRF-RX (4) is reduced to be

$$\begin{aligned} y_{BB}(t) &= y_{BB,I}(t) + j \cdot y_{BB,Q}(t) \\ &= a_1 \cdot x(t) + 3a_3 \cdot A^2(t) \cdot x(t) \end{aligned} \tag{6}$$

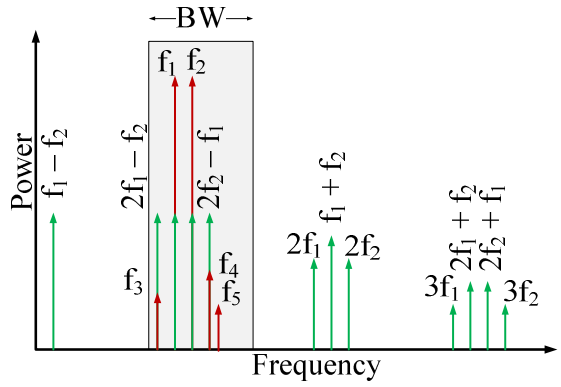

Fig. 3. Distribution of the distortion frequencies according to model in (5)

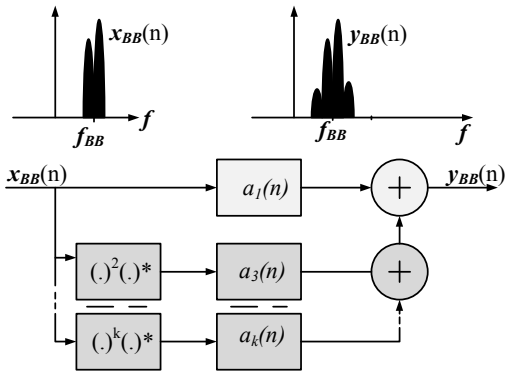

Fig. 4. A reduced non-linear model of LNA in multi-channel DRF-RXs after the DDC.

where,

$$y_{BB,I}(t) = a_1 \cdot x_I(t) + 3a_3 \cdot A^2(t) \cdot x_I(t) \tag{7}$$

$$y_{BB,Q}(t) = a_1 \cdot x_Q(t) + 3a_3 \cdot A^2(t) \cdot x_Q(t) \tag{8}$$

From (7)–(8), the distortion model at the baseband is much simpler compared to the model in the RF domain. The non-linear component $3a_3 \cdot A^2(t) \cdot x(t)$ essentially causes intermodulation in the frequency range around ω_c. The corresponding non-linear model and an example spectrums are illustrated in Fig. 4. Ideally, all high order-component are filtered by DDC and the spectrum of $x_{BB}(t)$ are shown in the left. However, due to the effect of intermodulation, the actual baseband spectrum (y_{BB}(t)) is shown in the right where new third-order distortions components appear near the interested frequencies.

To verify and simulate the effect of the models in (7)–(8), we set up a DRF-RX configuration with the carrier frequency of $\omega_c = 1$ GHz and three QPSK inputs: $f_{1,BB} = 9.5\,MHz$, $f_{2,BB} = 20.0\,MHz$, and $f_{3,BB} = 30.5$ MHz. After down-converting to the baseband with 100 Msps sampling rate (bandwidth of 50 MHz), the spectra of the signals including linear component and nonlinear distortions according to the models in (7)–(8) are shown in Fig. 5. From the figure, all three baseband signals are distorted by not only themselves but also by the adjacent channels

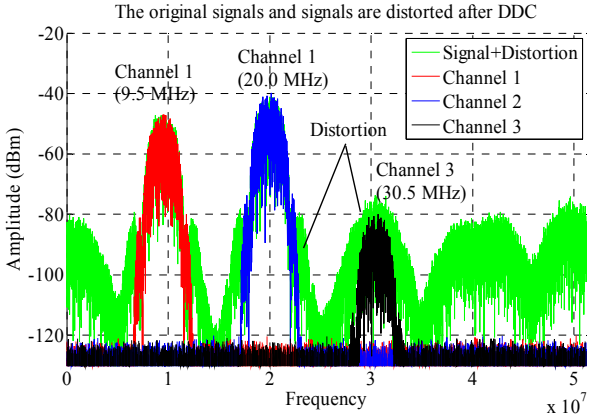

Fig. 5. Distortion due to the LNA nonlinearity with 3 QPSK signal channels of $f_{1,BB} = 9.5\ MHz$, $f_{2,BB} = 20.0\ MHz$, and $f_{3,BB} = 30.5$ MHz.

The derived models (7)–(8) in this Section will be used as the fundamental ground for designing the distortion compensation circuit for the DRF-RXs, which is presented in the subsequent Section.

III. Proposed Distortion Compensation Scheme For Multichannel DRF-RXs

A. Distortions Compensation Circuits

In this section, we propose a novel after-DDC distortion compensation scheme for DRF-RX. The structure of the proposed RX consists of a main receiver and a reference receiver depicted in Fig. 6. The former still needs an LNA to ensure good sensitivity as discussed before, while the latter is designed without LNA so that the received signals remain linear. This structure is similar to the design approach in [10] However, by exploiting the characteristics of a purely digital RXs and based on the model in (6)-(8), we shift all signal processing to the low-frequency domain after DDC and this brings a number of advantages. First, the digital downconverter practically adds no extra noise components (as opposed to the analog downconverter) and it helps to eliminate all even-order components and high-frequency components in (1). Furthermore, processing at a low-sampling rate, from the circuit design perspective, remarkably reduces the design complexity, cost and makes the overall system more energy- and area-efficient.

As can be seen from Fig. 6, both the RF signals of the primary and secondary receivers are converted to low frequencies by the same digital I/Q rails using two DDCs. A delay block is inserted behind the DDC1 in the main channel for synchronizing the two receivers because the reference receiver signal is slightly slower than the main one. The delay value, which depends on the timing characteristics of the distortion cancelation circuit, can be precisely tuned during the design phase. During distortion removal processing, harmonic and intermodulation components are regenerated by a reference receiver and will be used for subtracting the distortion component from the main receiver signal. The LMS algorithm is adopted in this scheme to estimate the appropriate coefficients a_{i} in (6). This process is analytically explained in the following.

Assuming the baseband signal received from the antenna after going through LNA, ADC and DDC is

$$\begin{aligned} y_{BB}[n] &= w_1[n] \cdot f_1(x_{BB}[n]) + w_3[n] \cdot f_3[n] \cdot (x_{BB}[n]) \\ &= x_{BB}[n] + e[n] \end{aligned} \tag{9}$$

where n is sampling sequence number, $f_1(x_{BB}[n]) = x_{BB}[n]$ is the linear component and $f_3(x_{BB}[n]) = x_{BB}^3[n]$ is the third-order components. $w_i[n]$ is the i$^{\text{th}}$-order coefficient. Accordingly, the distortion components in (9) are

$$e[n] = w_3[n] \cdot f_3(x_{BB}[n]) \tag{10}$$

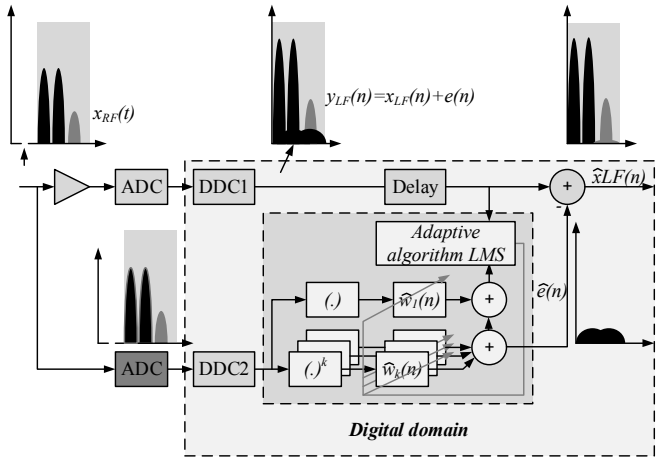

Fig. 6. The structure of multichannel DRF-RXs with the proposed distortion compensation circuit

From the linear reference channel, the reproduced distortion $\hat{e}[n]$ is expressed as

$$\hat{e}[n] = \hat{w}_3[n] \cdot f_3(x_{BB}[n]) \tag{11}$$

The distortion canceling circuit (see Fig. 6) subtracts the reproduced distortion components of the linear channel from the distorted signal after the main receiver DDC, hence

$$\hat{x}_{BB}[n] = y_{BB}[n] - \hat{e}[n] \tag{12}$$

From (9), (11) and (12) the final output signal is rewritten as

$$\begin{aligned} \hat{x}_{BB}[n] &= x_{BB}[n] + e[n] - \hat{e}[n] \\ &= x_{BB}[n] + (w_3[n] - \hat{w}_3[n]) \cdot f_3(x_{BB}[n]) \end{aligned} \tag{13}$$

From (13) it can be seen that the signal after distortion compensation $\hat{x}_{BB}[n]$ is equal to $x_{BB}[n]$ as long as high-order coefficients $\hat{w}_3[n]$ in (8) are the same as those $w_3[n]$ in (7). By adopting the LMS algorithm, the coefficients of the nonlinear model are determined as follows:

$$\begin{aligned} \hat{w}_1[n] &= \hat{w}_1[n-1] + \mu_1 \cdot f_1(x[n]) \cdot \hat{\varepsilon}[n] \\ \hat{w}_3[n] &= \hat{w}_3[n-1] + \mu_3 \cdot f_3(x[n]) \cdot \hat{\varepsilon}[n] \end{aligned} \tag{14},$$

where $\hat{\varepsilon}[n]$ and μ_i $\{i = 1 - 3\}$ are LMS algorithm parameters; $\hat{\varepsilon}$ is estimation error and is expressed as $\hat{\varepsilon}[n] = y[n] - \left(\hat{w}_1 \cdot f_1(x[n]) + \hat{w}_2 \cdot f_2(x[n]) + \hat{w}_3 \cdot f_3(x[n])\right)$; μ_i are the LMS algorithm step sizes. Fig.7. shows that the coefficients in the model are asymptotically converged to the actual nonlinear coefficients of LNA. Convergence time of $\hat{w}_i$ essentially is inversely proportional to the the step size μ_i as shown in Fig. 7. In our particular design and test case, the coefficient is converged after about 12×10^6 samples, just within a few seconds. Also from the figure, the simulation results indicate that the higher the convergence speed, the larger the error $\hat{e}[n]$

is. The latter eventually affects the performance of the compensation circuit. For further simulation we set μ_1, μ_2, and μ_3, are 1.25×10^{-6}, 2.5×10^{-6} and 5.0×10^{-6} respectively, which results in reasonable fast convergence speed and precision.

B. Evaluation of The Proposed Scheme

To evaluate the effectiveness of the proposed scheme, we have implemented a Matlab model for a DRF-RX which operates at UHF (300 MHz–3 GHz) with a reception bandwidth of 50 MHz and can simultaneously receive several dozens of channels with the local bandwidth of 2 MHz. This configuration is set accordingly to some practical applications such as voice and data cellular networks, over-the-air television, digital television, etc [23].

To estimate the SFDR value at baseband, we adopted the standard method in [20] by setting signal inputs of the receiver to be 2-tone, separated by 2 MHz. After the downconverter, the received tones at baseband are $f_1 = 9.5$ MHz and $f_2 = 11.5$ MHz with signal spectra before and after the distortion correction is shown in Fig. 8. From the figure, the SFDR increases almost by 30 dB for the RXs with compensation circuit, compared to the conventional one.

Furthermore, to evaluate BER, we have set three QPSK channels with a 4 Mbps data rate and the input scenario described in Section IIII.B (i.e., the carrier frequency is 1 GHz, baseband frequency are $f_{1,BB} = 9.5$ MHz, $f_{2,BB} = 20$ MHz, and $f_{3,BB} = 30.5\ MHz$). The input power levels of f_1 and f_2 are intentionally set to be -50 dBm and -43 dBm, which are higher than f_3 (-83 dBm). Thus, f_1 and f_2 will act as the aggressor channels. Intermodulation distortions from these two channels will appear around f_1, f_2 themselves and also around f_3. The spectrum for the distorted signals and the corrected signals is shown in Fig. 9. As can be seen, the spectra of corrected signals are mostly the same as the spectra of the original signals shown in Fig. 5. The nonlinear components generated by f_1 and f_2 are effectively reduced close to the noise floor.

Furthermore, to evaluate the proposed circuit by the BER, two RX configurations, with and without distortion compensation circuit were simulated. The BERs for both RXs were estimated based on 4 million received samples after demodulation, the digital input data was randomly generated. The results show that BER of RX without distortion compensation for channel f_3 is 0.38, which is unusable even for audio communication purposes. For the RX with applying the proposed compensation, the BER of f_3 channel is greatly improved to be 1.25×10^{-4}, i.e., reduces by three orders of magnitude. This confirms that our proposed scheme effectively removes the distortions and recovers the useful signal.

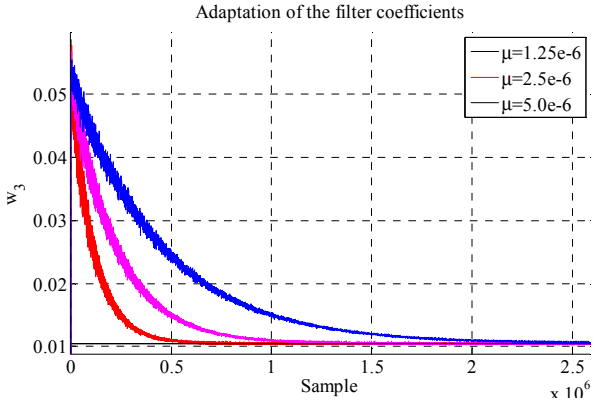

Fig. 7. Convergence characteristics of the third-order coefficient of the nonlinear model in using different LMS step size μ.

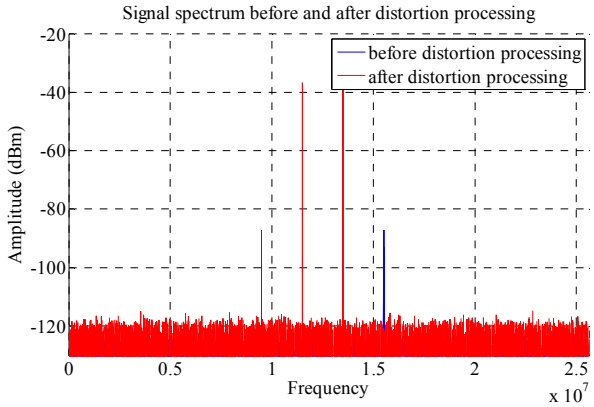

Fig. 8. Two-tone signal spectrum before and after distortion processing for estimating SFDR.

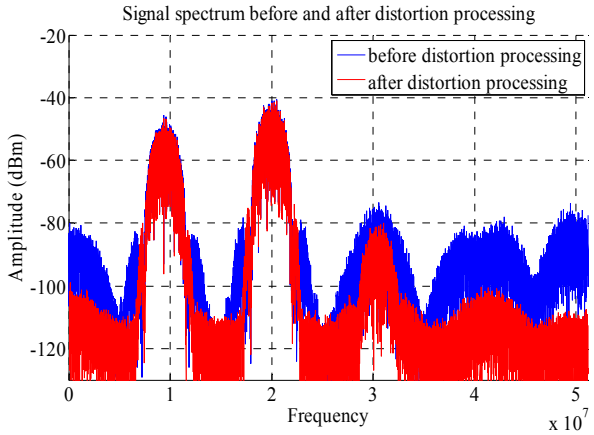

Fig. 9. Simulated spectra of the signals before and after compensation for UHF DRF-RXs (carry frequency of 1 GHz, baseband frequency are $f_{1,BB} = 9.5$ MHz, $f_{2,BB} = 20$ MHz, and $f_{3,BB} = 30.5\ MHz$).

IV. CONCLUSIONS

In this paper, the impacts of LNA distortions on DRF-RXs have been systematically studied in detail. From the derived signal analytical models, we have proposed a novel distortion compensation scheme for DRF-RXs that allows shifting all processes into the low-frequency domain. The proposed technique has been fully implemented and verified by Matlab simulation for a typical input scenario and RX configuration. The simulation for the two-tone signal showed an increase of ~30 dB signal SFDR compared to that of the conventional design. Furthermore, a test case of 3 QPSK signal inputs showed not only the visible improvement in the spectrum of

the received signal but substantially reductions of ~1000 times in BER.

The proposed compensation scheme also exhibits a great advantage in power consumption and the design cost and design complexity because the signal processing is done entirely in the low-sampling rate. The proposed RX design hence is very practical and well-suited for applications such as mobile, portable and handheld communication devices, where both energy consumption and design cost are the major concerns.

ACKNOWLEDGEMENT

This research is funded by Vietnam National Foundation for Science and Technology Development (NAFOSTED) under grant number 102.01-2018.310

REFERENCES

[1] Software Defined Radio, Spectrum Analyzer, and Panoramic Adapter/ Available: http://www.rfspace.com/RFSPACE/SDR-IQ.html. [Accessed May 20, 2019].

[2] Perseus SDR - Software Defined 10 kHz - 30 MHz Receiver. Available: http://microtelecom.it/perseus/. [Accessed May 20, 2019].

[3] O. Jamin, *Broadband Direct RF Digitization Receivers*, Analog Circuits and Signal Processing 121, DOI 10.1007/978-3-319-01150-9_2, Springer International Publishing Switzerland 2014

[4] A. A. Abidi, "Direct-conversion radio transceivers for digital communications," *IEEE J. Solid-State Circuits*, vol. 30, no. 12, pp. 1399–1410, Dec. 1995.

[5] O. Jamin, V. Rambeau, F. Goussin, and G. Lebailly, "An rf frontend for multi-channel direct rf sampling cable receivers," in *2011 Proceedings of the ESSCIRC*, Sept 2011, pp. 347–350.

[6] B. Razavi, "Design considerations for direct-conversion receivers," *IEEE Trans. Circuits Syst. II, Analog Digit. Signal Process.*, vol. 44, no. 6, pp. 428–435, Jun. 1997.

[7] L. Anttila, M. Valkama, and M. Renfors, "Circularity-based I/Q imbalance compensation in wideband direct-conversion receivers," *IEEE Trans. Veh. Technol.*, vol. 57, no. 4, pp. 2099–2113, Jul. 2008.

[8] E. Bautista, B. Bastani, and J. Heck, "Improved mixer IIP2 through dynamic matching," *in IEEE Int. Solid-State Circuits Conf. Dig. Tech. Papers, San Fransisco, CA, USA*, Feb. 2000, pp. 376–377.

[9] R. Vansebrouck, O. Jamin, P. Desgreys, and V.-T. Nguyen, "Digital distortion compensation for wideband direct digitization RF receiver," *in Proc. IEEE 13th Int. New Circuits Syst. Conf. (NEWCAS),* Jun. 2015, pp. 1–4.

[10] Jaakko Marttila, Markus Allénand Marko Kosunen, "Reference Receiver Enhanced Digital Linearization of Wideband Direct-Conversion Receivers" *IEEE Transactions On Microwave Theory And Techniques*, vol.65, no. 2, pp. 607-620, February 2017

[11] M. Allén, J. Marttila, M. Valkama, S. Singh, M. Epp, and W. Schlecker, "Digital full-band linearization of wideband direct-conversion receiver for radar and communications applications," in *Proc. 49th Asilomar Conf. Signals, Syst. Comput.*, Pacific Grove, CA, USA, Nov. 2015, pp. 1361–1368.

[12] Raphaël Vansebrouck, Chadi Jabbour, Olivier Jamin, and Patricia Desgreys, "Fully-Digital Blind Compensation of Non-Linear Distortions in Wideband Receivers" *IEEE Transactions On Circuits And Systems-I: Regular Papers*, vol. 64, no. 8, pp. 2112-2123, August 2017.

[13] M. Grimm, M. Allen, J. Marttila, M. Valkama, and R. Thoma, "Joint mitigation of nonlinear rf and baseband distortions in wideband direct conversion receivers," *Microwave Theory and Techniques, IEEE Transactions on*, vol. 62, no. 1, pp. 166–182, Jan 2014.

[14] Gharaibeh, Khaled M, *Nonlinear distortion in wireless systems: modeling and simulation with MATLAB*, John Wiley & Sons Ltd, 2012

[15] Texas Instruments. "ADC32RF83 Dual-Channel, 14-Bit, 3-GSPS, RF Sampling Wideband Receiver, and Feed," ADC32RF83 datasheet Available: http://www.ti.com/product/ADC32RF83

[16] Texas Instruments. "ADC32RF45 Dual-Channel, 14-Bit, 3-GSPS RF-Sampling Analog-to-Digital Converter (ADC)," ADC32RF45 datasheet, Available: http://www.ti.com/product/ADC32RF45

[17] S. Haykin, *Adaptive Filter Theory*, 4th ed. Upper Saddle River, NJ, USA: Prentice-Hall, 2002.

[18] Why Oversample when Undersampling can do the Job?, https://www.analog.com/en/analog-dialogue/articles/adc-input-noise.html

[19] Leon Melkonian, *Improving AD Converter. Performance Using Dither*, National Semiconductor. Application Note 804. February 1992.

[20] Admoon Andrawes "Multi-tone Analysis in Nonlinear Systems," 2nd International Conference on Advances in Computational Tools for Engineering Applications (ACTE), pp. 96-100, 2012

[21] E1 Telecom: *A Global Communication Standard For Digital Voice Communication.* Available: https://www.dpstele.com/e1/index.php [Accessed May 20, 2019].

[22] Barakat, A., Thian, M., & Fusco, V. (2015). *Analysis of the Second Harmonic Effect on Power Amplifier Intermodulation Products*, In 2015 SBMO/IEEE MTT-S International Microwave and Optoelectronics Conference (IMOC) Institute of Electrical and Electronics Engineers (IEEE). Available: https://doi.org/10.1109/IMOC.2015.7369207 [Accessed May 20, 2019].

[23] Aselsan. "PRC V/UHF SDR Handheld Radios." Available: https://www.aselsan.com.tr/en-us/capabilities/military-communication-systems/v-uhf-military-radios/prc-v-uhf-sdr-handheld-radios